APPLICATION OF PASSIVE FLOW CONTROL DEVICE ON HELICOPTER ROTOR BLADES

F. Tejero, P. Doerffer, O. Szulc
The Szwealski Institute of Fluid-Flow Machinery
Polish Academy of Sciences
Fiszera 14, Gdansk, 80-231, Poland
email: fernando.tejero@imp.gda.pl

Abstract. Application of an efficient flow control system on helicopter rotor blades may lead to improved aerodynamic performance. Recently, the own invention of a passive vortex generator (Rod Vortex Generator - RVG) has been analysed for channel and wing flows proving its capability to reduce flow separation. The application of this passive flow control device on helicopter rotor blades is described in the present paper. The basic flow mechanism is based on the intensification of exchange of momentum in the direction normal to the wall by a streamwise vortex. High momentum air is transferred to the low momentum region close to the surface and therefore the separation bubble is reduced. The present CFD investigation was carried out with the FLOWer code from DLR which solves the Favre-averaged Navier-Stokes equations using the chimera overlapping grids technique and LEA (Linear Explicit Algebraic Stress) k-ω turbulence model. The validation of the numerical set-up for high-speed transonic hover conditions is based on a comparison with experimental data obtained by Caradonna and Tung (1981). For forward flight regime, the validation is based on a comparison with flight test data gathered by Cross and Watts for the AH-1G helicopter (1988). It has been proven that the application of the proposed flow control system reduces the size of the separation bubble increasing the aerodynamic performance in both states of flight.

Nomenclature

Symbols

c	blade chord (m)
d	rod diameter (m)
h	rod height (m)
L	spacing between vortex generators (m)
M	Mach number (-)
M_T	tip Mach number (-)
M_∞	forward flight Mach number (-)
Re_T	tip Reynolds number (-)
r	rod radius (m)
V_∞	forward flight velocity (km/h)
C_f	skin friction coefficient (-)
C_P	blade pressure coefficient (-)
C_{P0}	rotor power coefficient (-)
C_Q	rotor torque coefficient (-)
C_T	rotor thrust coefficient (-)
α	rod skew angle (˚)
β_c	backward disk tilt (˚)
β_s	sideways disk tilt (˚)
δ	boundary layer thickness (m)
μ	rotor advance ratio (-)
θ_0	blade collective angle (˚)
θ_c	lateral cyclic coefficient (˚)
θ_s	longitudinal cyclic coefficient (˚)
Θ	rod pitch angle (˚)
ψ	blade azimuthal position (˚)

Abbreviations

C-T	Caradonna and Tung
FC	Flow Control
RVGs	Rod Vortex Generators
VGs	Vortex Generators

1. INTRODUCTION

Flow separation control is essential in many technological applications. One of the most popular flow control systems are vortex generators (VGs). Conventional passive vane vortex generators have been used for separation control for many years. Proposed by Taylor[1] at the end of the 40s, VGs have been used, among other purposes, to delay boundary-layer separation[2], to enhance aircraft wing lift[3] or to control separation in subsonic diffusers[4]. Main drawback of these configurations was an excessively large height ($h \approx \delta$) of the vortex generators inducing a considerable drag penalty. An alternative manner to induce streamwise vortex by air jets was proposed in the 50s by Wallis[5,6]. The streamwise vortex is formed by the interaction between the free stream flow and air jet avoiding the appearance of a parasitic drag. During last decades, several experimental[7,8] and numerical[9,10] investigations proved that this technology is effective in delaying flow separation and improving the aerodynamic performance of airfoils.

The research conducted by Rao and Kariya[11] in the 80s suggested that low-profile vane vortex generators (h/δ<0.625) exceed the performance of conventional VGs (h≈δ). Over the last years, different researchers have analyzed the influence of the height and shape of vortex generators. A review of the state of the art concerning low-profile vortex generators applied to flow separation control was conducted by Lin[12]. As alternative streamwise vortex generator, Doerffer[13] introduced the rod vortex generators in 2009. The own invention of passive flow control system has been analyzed in channel flows (shock wave-boundary layer interaction at M=1.43) proving its capability to reduce flow separation. Rod vortex generators are defined by 5 parameters: diameter (d), height (h), spacing between rods (L), skew angle (α) and pitch angle (Θ) - see fig.1a. According to the previous investigations, it was concluded that the first three parameters should be proportional to the boundary layer thickness while the optimum values of the skew and pitch angles for inducing the strongest streamwise vortex are 45˚ and 30˚ respectively. As an example, figure 1b presents the contour map of streamwise vorticity in a cross-section downstream of an isolated and deployed rod.

As a step forward, the application of the proposed vortex generators on helicopter rotor blades is being studied. The severe flow conditions existing (i.e. shock wave-boundary layer interaction on the advancing side and dynamic stall on the retreating side for forward flight conditions) suggest this technology as a possible candidate to be integrated in the next generation of helicopters. Two states of flight are considered in this paper: hover and forward flight. For validation purposes, the Caradonna and Tung[14] model helicopter rotor is simulated and the numerical results are compared against the experimental data. On the other hand, a validation of the numerical set-up for forward flight conditions is based on the comparison with flight test data obtained by Cross and Watts for the AH-1G helicopter[15]. For both cases, the application of rod vortex generators is analysed (flow control cases).

2. PHYSICAL AND NUMERICAL MODELLING

2.1 FLOWer Code from DLR

The present CFD investigation was carried out with the FLOWer[16] solver from DLR. It is a modern, parallel, block-structured, cell-centered code solving the Favre-averaged Navier-Stokes equations with several turbulence models. The two-equation, low-Reynolds number model, Linear Explicit Algebraic Stress model[17] (LEA k-ω) was used for the numerical investigation due to improved prediction capabilities for transonic flows. Additional benefit for chimera overlapping grids technique is lack of the wall distance calculation in the closure. The numerical algorithm is based on a semi-discrete approach with a finite-volume, central scheme of 2nd order of accuracy for the spatial discretization.

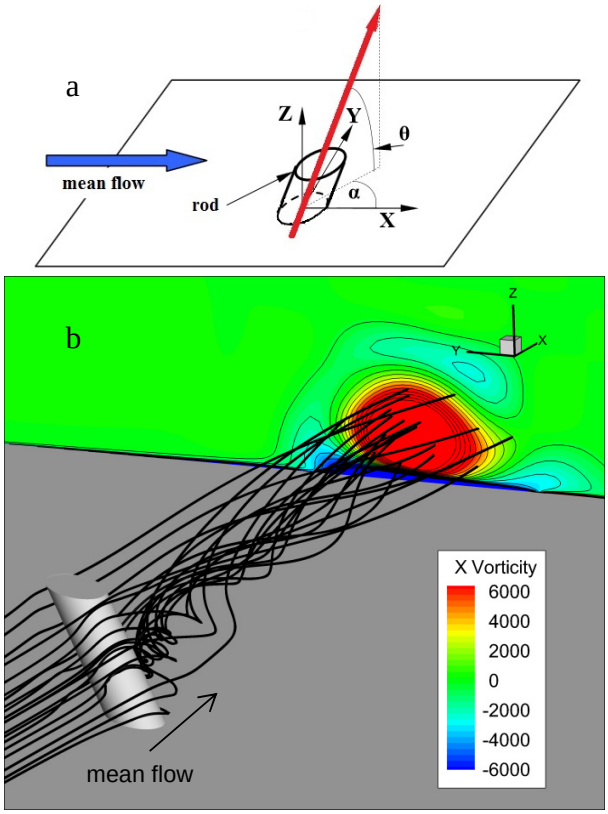

Figure 1. (a) RVG schematic view (b) Isolated RVG inducing streamwise vortex

The same explicit, Runge-Kutta method (CFL = 2.5) of time integration was used for steady state numerical simulation of a hovering rotor, as for the internal iterations of the time-accurate implicit dual-time-stepping scheme of 2nd order accuracy for forward flight conditions. For the steady state (hover), the convergence criteria was based on a reduction of density residual by 6 orders of magnitude and stabilization of C_T and C_Q coeffcients. For the forward flight simulation, the time needed for a rotation by 0.25˚ of azimuth was chosen for the time step (1440 time steps per revolution). At each physical time step, a drop of density residual by 3 orders of magnitude proved to be sufficient to obtain accurate unsteady flow-field around the rotor.

2.2 Chimera Component Grids

The ROT version of the FLOWer code allows to use the chimera overlapping grids technique[18]. The main idea of the chimera technique is to generate easily grids for complex configurations by decomposing them into simple, independent parts. The only limitation is that all component meshes should overlap each other to allow inter-grid communication. This technique is appropriate for computing helicopter rotor blades. For hover conditions, a constant collective is applied. In case of forward flight the chimera overlapping grids technique allows for an easy control of the rigid motion of the blades (translation, rotation, pitch and flap) preventing any grid deformation.

The component overlapped grids for the C-T and AH-1G rotor blades are generated semi-automatically using parameterized python scripts within the IGG (Numeca International) software. For the reference cases (no flow control) the domain is formed by background and blade component grids. For the flow control cases, the vortex generators component grid is added to the reference set-up. For hover computations, the background component grid is a cylinder of a height equal to 6.1 R and radius of 4.0 R which ensures that the rotor blades are located, at least, 3.0 R from the outer part of the domain. Altogether 32 computational blocks contain $4.80 \cdot 10^6$ volumes. The vicinity of the rotor and its wake is solved with a cuboid structure with uniform volumes (0.1c × 0.1c × 0.1c). For forward flight simulations, a Cartesian background (see figure 2) is designed with dimensions of 16.4 R × 18.2 R × 18.2 R, consequently the outer part of the domain surface is located at least 8.0 R away from the rotor in every direction.

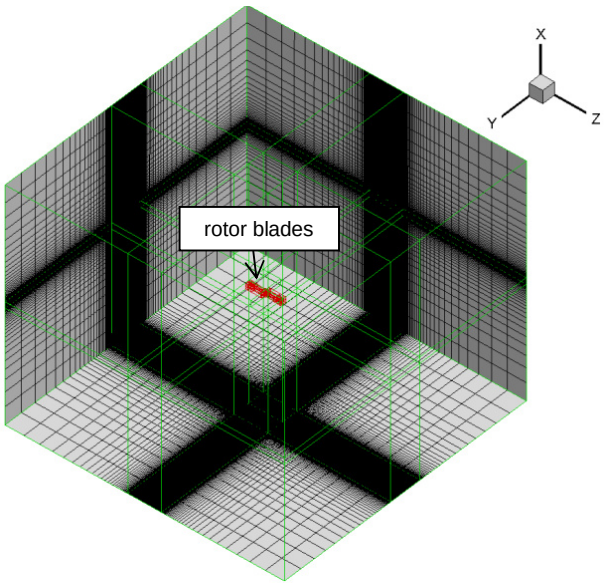

Figure 2. Background component grid

The number of blocks is the same as for the hover case but the number of volumes is increased up to $9.4 \cdot 10^6$. The vicinity of the rotor is solved with a cuboid structure with uniform volumes (0.1c × 0.1c × 0.1c) as well.

For both states of flight, the blade grid (fig. 3) is of C-type in streamwise and H-type in crosswise direction. It spans from the surface 1.2 c in all directions (radial and normal). Altogether 40 computational blocks contain $3.9 \cdot 10^6$ of volumes per blade. The non-dimensional distance of the first layer of cells from the solid surface of the blade is of the order of $y^+ = 1$ for hover and forward flight conditions, which is sufficient for resolving the laminar part of the turbulent boundary layer using low-Re turbulence model of LEA k-ω.

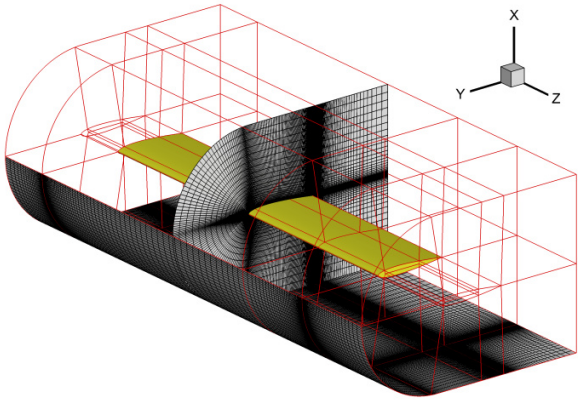

Figure 3. Single blade component grid

Three types of boundary conditions are applied in the numerical simulation: no-slip condition with zero heat-flux (adiabatic) at the rotor blades, Froude[19] (hover case) and far-field conditions (forward flight case) at the edge of the background grids and a special chimera condition at the outer edge of the blade component grids which is necessary for the interpolation of the flow variables between meshes.

For the flow control cases, a vortex generator component grid is added to the chimera setup. It is located at the suction side of the blade where there is significant flow separation. Number of rods and their dimensions are defined according to the numerical results of section 3. Figure 4 presents the block topology of the VGs component grid (the figure refers to the mesh formed by 14 rods implemented in hover computations).

Table 1 summarizes the number of blocks and volumes of the computational grids designed for simulation presented in the paper. The inclusion of rods component grid leads to a significant increase of

the mesh size making the simulation computationally demanding ($37 \cdot 10^6$ - $48 \cdot 10^6$ volumes).

	No. of blocks	No. of volumes
C-T hover - ref.	114	$12.7 \cdot 10^6$
C-T hover - FC	616	$36.7 \cdot 10^6$
AH-1G forward flight - ref.	114	$17.3 \cdot 10^6$
AH-1G forward flight - FC	748	$47.6 \cdot 10^6$

Table 1. Computational grids (ref – reference case, FC – flow control case)

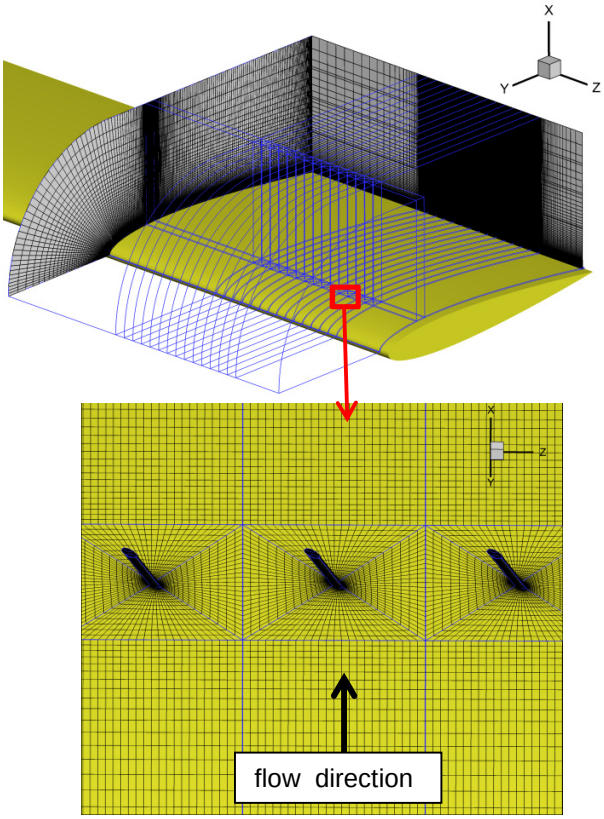

Figure 4. RVGs component grid

3. VALIDATION OF THE NUMERICAL METHOD

3.1 Caradonna-Tung Model Helicopter Rotor in High-Speed Hover

The experimental data obtained by Caradonna and Tung[14] is the first test data available in the literature that combines measurements of blade loading and tip vortex trajectory. This 2-bladed model helicopter rotor is very popular within the rotorcraft community serving for validation of CFD codes. The high-speed transonic hover conditions with a tip Mach number of 0.877 and collective equal to 8° assures strong shock waves close to the tip which induce flow separation. A literature survey of the RANS results obtained for this transonic lifting hover case reveals significant scatter according to the experimental data[20-23]. However, the FLOWer prediction of this transonic flow-field is acceptable as one of the better RANS solution that can be found in the literature so far. The authors of the present paper have been dealing with this severe test case using different physical models (steady and unsteady), numerical grids (block-structured and chimera), flow solvers (SPARC, FLOWer and NUMECA) and turbulence models (i.e. Spalart-Allmaras) with success[24,25] in the past.

One of the most important aspects of hover computations is a proper prediction of the rotor wake. A strong induced vertical inflow modifies the effective angle of attack of the blades altering the rotor performance. As an example, figure 5 presents the wake structure (Q-criterion colored by vorticity magnitude) revealing contracting and descending helical shape. The grid refinement is sufficient for capturing the first rotor revolution (first passage of the tip vortex below the preceding blade).

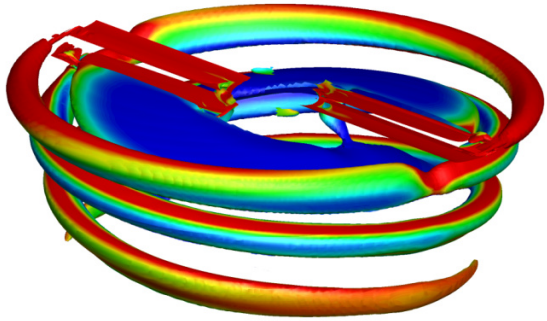

Figure 5. Aerodynamic wake of the C-T rotor

The validation of the numerical method presented in figure 6 is based on the comparison of the pressure coefficient distributions C_p at five cross-sections along the span of the blade (r/R = 0.50, 0.68, 0.80, 0.89, 0.96). High tip Mach number and collective angle of the blades induce supersonic areas terminated by shock waves at the three outer sections. The shock location is predicted correctly by the FLOWer solver. The slight deviation between CFD and experimental data integrated over the whole surface of the blade leads to an overprediction by 15% (C_T = 0.00545) of the measured thrust coefficient (C_T = 0.00473). It is important to mention that the reason of this discrepancy may lay in the integration method of C_p cross-sections (coarse) which is not explained in the experimental description. A large amount of thrust is generated between the last measured cross-section (r/R = 0.96) and the tip. Therefore, lack of the experimental values of C_p for r/R > 096 reduced the

accuracy of the post-processing of the measured data in terms of thrust coefficient. The size of the separation bubble (streamlines highlighted in white color) at the suction side of the blade is presented in figure 6. The length of the reverse flow area in spanwise direction is almost 0.1 R (from r/R = 0.86 to 0.96) with a detachment point constantly located at the chordwise station x/c = 0.30. It is at r/R = 0.92 where the most severe reverse flow appears with a length of the separation bubble equal to 15% of the chord. The boundary layer thickness (δ) upstream of the shock wave was approximately 0.008 c. According to previous investigations[26], the rods were designed with the following parameters: ϕ = δ/4, h = δ/2 and L = 2.5 · δ. The spacing between the rods was increased to L = 5 · δ (instead of L = 2.5 · δ) in order to reduce the number of volumes of the computational grid (still very computationally demanding test case). A description of the numerical implementation of RVGs for a hovering helicopter blade is shifted to section 4.

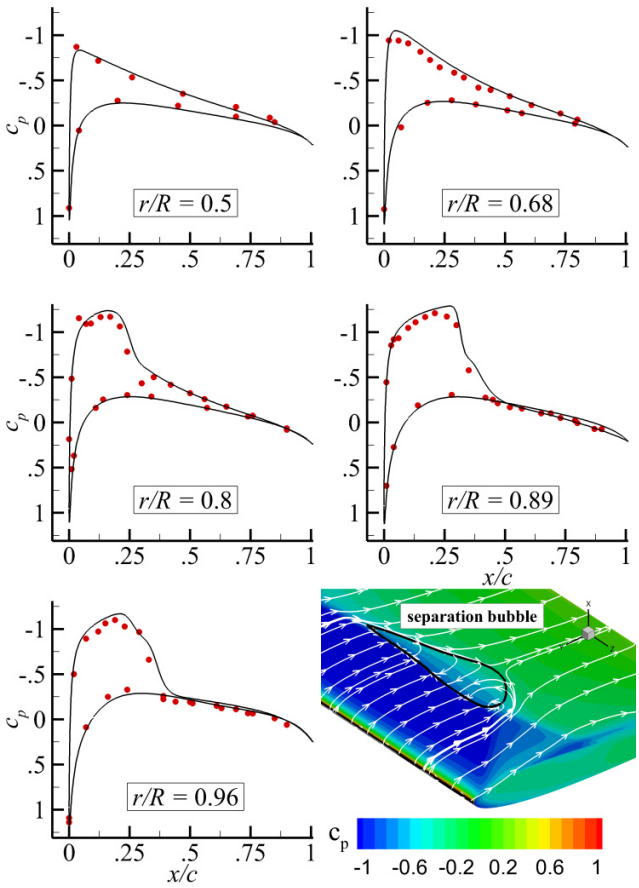

Figure 6. Pressure coefficient distribution (C_p) and separation bubble (C-T rotor)

3.2 AH-1G Helicopter Rotor Blade in Forward Flight

The flight test data obtained by Cross and Watts[15] for the AH-1G helicopter is one of the most detailed data bases that can be found in the open literature. It combines aerodynamic (i.e. normal forces or C_P distributions) and aeroacoustic data. The rotor is a two-bladed rectangular-planform teetering rotor with the Operational Loads Survey (OLS) symmetrical airfoil section and a linear twist of -10° from the root to the tip. During the flight test the instantaneous values of the rotor control angles were recorded (pitching, flapping and shaft angles) and are applied in the simulations. Various numerical approaches/methods have been carried out over the last years concerning this helicopter rotor. Hernandez and Johnson[27] used the CAMRAD/JAFPR code including a rotor wake model. Ramachandran et al.[28] developed a method based upon the vorticity-embedding technique. Ahmad and Duque[29] applied the chimera method to allow the blade motion in their research. For the present investigation[30], a low-speed (test point 2157), medium-speed (test point 2155) and high-speed case (test point 2152) have been considered. Table 2 summarizes the flow conditions for each test case. In contrast to the low-speed case, the numerical results for the medium- and high-speed flights are unique in terms of the literature survey.

	low-speed	medium-speed	high-speed
M_T [-]	0.65	0.65	0.64
Re_T [-]	$9.72 \cdot 10^6$	$9.78 \cdot 10^6$	$10.22 \cdot 10^6$
M_∞ [-]	0.12	0.17	0.24
V_∞ [km/h]	150	210	295
μ [-]	0.19	0.26	0.38
θ_0 [°]	11.7	13.4	18.0
θ_c [°]	1.7	2.1	3.6
θ_s [°]	-5.5	-7.9	-11.8
β_c [°]	2.13	2.38	1.13
β_s [°]	-0.15	0.19	1.11
C_T [-]	0.00464	0.00464	0.00474

Table 2. Flight test flow conditions and blade motions

The blade motion is imposed according to the flight test data of table 2 in a form of a Fourier series using the first harmonics (eq.1 and 2). The value of the collective pitch θ_0 is referred to the cross-section r/R = 0.75.

(1) $\theta = \theta_0 + \theta_c \cdot \cos(\psi) + \theta_s \cdot \sin(\psi)$

(2) $\beta = \beta_0 + \beta_c \cdot \cos(\psi) + \beta_s \cdot \sin(\psi)$

As an example, the predicted normal force coefficient respects the azimuth at r/R = 0.86 for low- and medium-speed cases is presented in figure 7. The agreement between CFD and flight test data is satisfactory for the low-speed case (C_T is overpredicted by 2%). Although more discrepancies appear for the medium-speed case (C_T is overpredicted by 9.3%), the fit is still acceptable. Finally, the thrust coefficient is overpredicted by 20% for the high-speed case. The agreement with flight test data is acceptable taking into account the complexity of the flow: strong shock wave at the advancing side and massive flow separation at the retreating side due to dynamic stall. Similar deviation in thrust was obtained for a high-speed flight of the 4-bladed rotor of the PZL W-3A "Sokół" (Falcon) helicopter[31] using similar model.

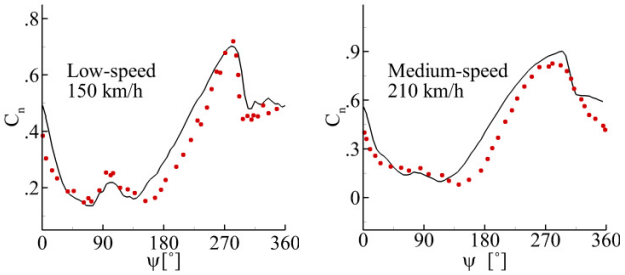

Figure 7. C_n comparison for low- and medium-speed at r/R=0.96 (AH-1G rotor)

Out of three test flights analyzed, only the high-speed case reveals significant flow separation possible to be controlled by the rod vortex generators. The complex wake structure presented in figure 8 (Q-criterion colored by vorticity magnitude) is a consequence of severe flow conditions.

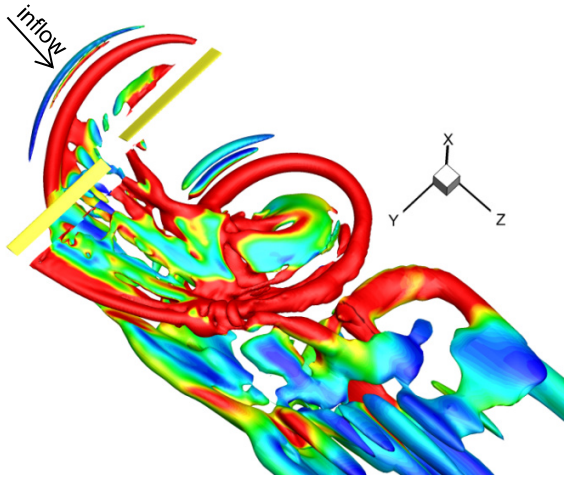

Figure 8. Aerodynamic wake of the AH-1G rotor in high-speed forward flight

Figure 9 presents a contour map of the skin friction coefficient (C_F) at the suction side of the blade in steps of 30˚ of rotation. The blue color refers to location where the flow is attached to the blade surface, the red color represents reverse flow areas and the green zones are locations where the flow is attached to the blade surface exerting low shear stress (the flow is almost separated). It is worth to mention that near ψ = 30˚ there is local flow separation induced by the shock wave. On the other hand, there is flow separation at the retreating side close to ψ = 270˚ due to high angle of attack. It is important to remark that this kind of visualization cannot distinguish between areas of boundary layer separation and reserved flow due to difference between rotational and forward speeds.

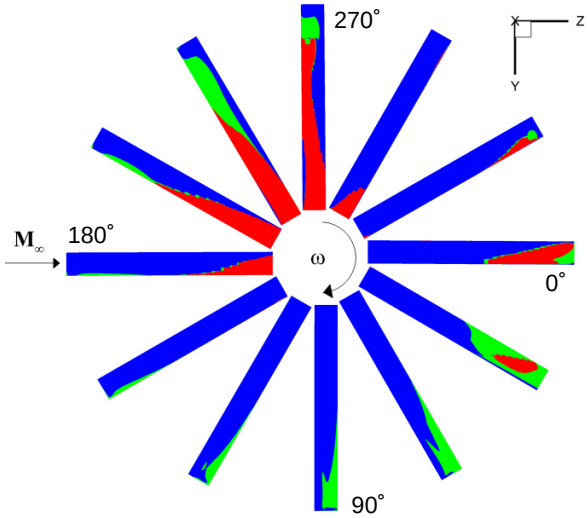

Figure 9. Sign of skin friction coefficient (C_f) for high-speed forward flight (AH-1G rotor)

Figure 10 presents contour map of the pressure coefficient at the suction side of the blade in steps of 30˚ of rotation. A strong shock wave at the advancing side (before ψ = 90˚) and dynamic stall at the retreating side appear for these flow conditions. The normal force coefficient versus the azimuth at r/R = 0.86 and 0.96 is presented as well. The overprediction by 20% of the thrust coefficient leads to a similar overestimation of normal force. Finally, pressure coefficient distributions at two representative azimuthal positions (advancing – a1 and retreating – r1 sides) are also presented in figure 10. The shock wave location and the pressure coefficient distribution in the area of dynamic stall are well reproduced by CFD.

The design of the rod vortex generators for this forward flight case is more challenging compared to

hover conditions because the flow properties are varying continuously and therefore the separation bubble size (width, length…) is not stable in time. In this case, the rods were designed according to the properties of the flow upstream of the shock wave that starts to appear at ψ = 30˚. In total 18 rod vortex generators covered the span of the blade between r/R = 0.91 and r/R = 0.96. It ensures that the rods will influence the flow where shock wave is present and partially affect the flow where dynamic stall occurs. As a next step, rod vortex generators will be placed in the inner part of the blade in order to study their influence at the retreating side of the rotor where massive flow separation appears due to low speed dynamic stall. The boundary layer upstream of the shock wave at ψ = 30˚ was approximately 0.004 c. As for the hover case, the rods were designed with the following parameters: ϕ = δ/4, h = δ/2 and L = 5 · δ. It is expected that the application of rods improves the aerodynamic performance by limiting flow separation induced by the shock wave (near ψ = 30˚) and shrinking the regions of low shear stress present between ψ = 30˚ and ψ = 270˚.

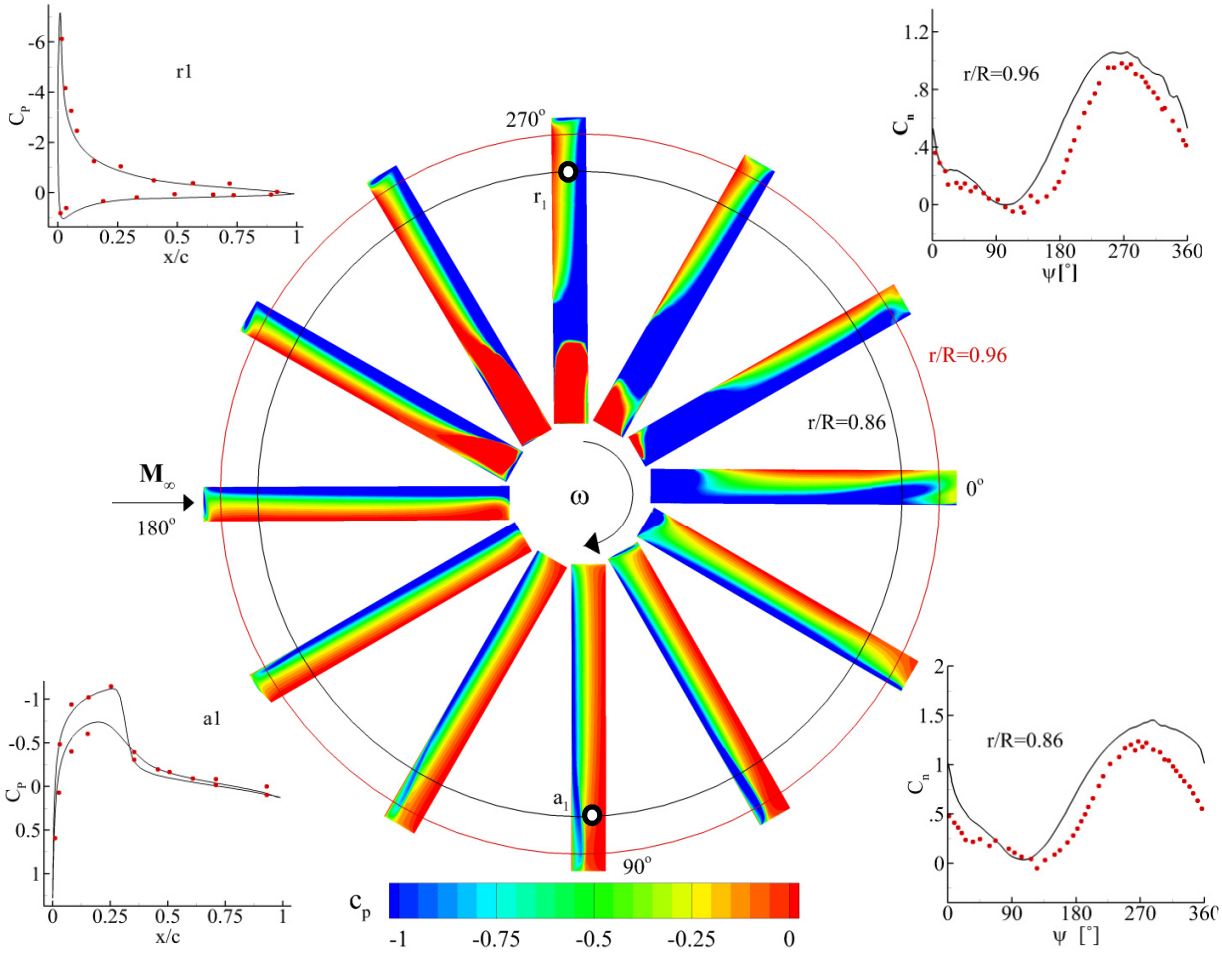

Figure 10. Pressure coefficient distribution (C_p) and normail force coefficient C_n for the high-speed flight of AH1G

4. IMPLEMENTATION OF ROD VORTEX GENERATORS ON HELICOPTER ROTOR BLADES

4.1 C-T High-Speed Hover Case with RVGs

The implementation of rod vortex generators at the suction side of the C-T model helicopter rotor blade in hover leads to a creation of strong streamwise vorticity. This effect is only visible below the edge of the boundary layer where VGs are submerged. The post-processing of the numerical simulation reveals that the vortex core develops and increases its intensity until flow separation where it is lifted and strongly dissipated.

The formation of streamwise vorticity increases the shear stress and attracts the flow towards the blade. As a consequence, the boundary layer profiles become fuller. This phenomenon stabilizes the flow

and therefore separation can be controlled. In figure 11 boundary layer profiles are compared for two cross-sections (reference against flow control case). The solid line represents the location downstream of one of the RVGs (S1 at r/R=0.92) while the dashed line refers to a cross-section located between two rods (S2 at r/R=0.91). If the profile is on the left side of the vertical blue line, the flow is reversed. The application of the proposed flow control eliminates the flow separation at that specific location.

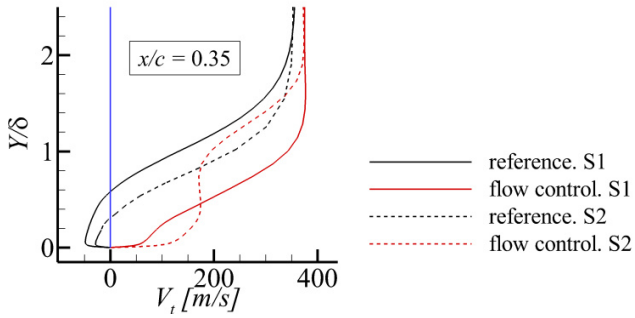

Figure 11. The effect of RVGs on the boundary layer developments.

The application of the proposed flow control device leads to decrease of the height of separation bubble. Figure 12 presents a contour map of skin friction coefficient (C_f) revealing the shape of the separation. The implementation of rod vortex generators leads to a noticeable increase of C_f due to the formation of streamwise vorticity and a reduction of the separation bubble area. Although the proposed configuration of rod vortex generators is not able to fully eliminate the reverse flow, the increase of the diameter/height of the rod (stronger streamwise vorticity but more drag penalty) or decrease of the spacing between the rods could attach the flow to the blade surface. The changes of the flow properties due to the implementation of rod vortex generators close to the tip of the C-T model rotor blade increase the thrust coefficient by 2% with respect to the reference case (no flow control). The main drawback of this flow control technology is the drag penalty which increases the power consumption (C_{P0}) of the rotor by 1%. Although the aerodynamic performance has been improved with the implementation of the flow control device, it is expected that more severe conditions would lead to a larger enhancement.

4.2 AH-1G High-Speed Forward Flight Case with RVGs

In contrast to the hover case, the inflow velocity and blade position (pitch, flap…) are continuously varying in forward flight. For this reason, the optimum approach for the implementation of a flow control device for such conditions would be to actively control it according to the requirements. As a first approach, the analysis of the proposed passive rod vortex generators will be performed for a constant deployment. Presented results are very valuable in terms of the potential benefits of this technology and possible drawbacks when it is used incorrectly. Figure 13 presents the AH-1G rotor disk loading for the reference high-speed (295 km/h) case. The majority of the lift is generated by fore and aft parts of the rotor disk with limited contribution from the advancing blade close to 90˚ and the retreating blade close to 270˚. The area of the reverse flow due to negative inflow velocity appears close to the root at the retreating side leading to a negative normal force coefficient (C_n). The negative pitch angle at the tip at the advancing side produces a negative force as well.

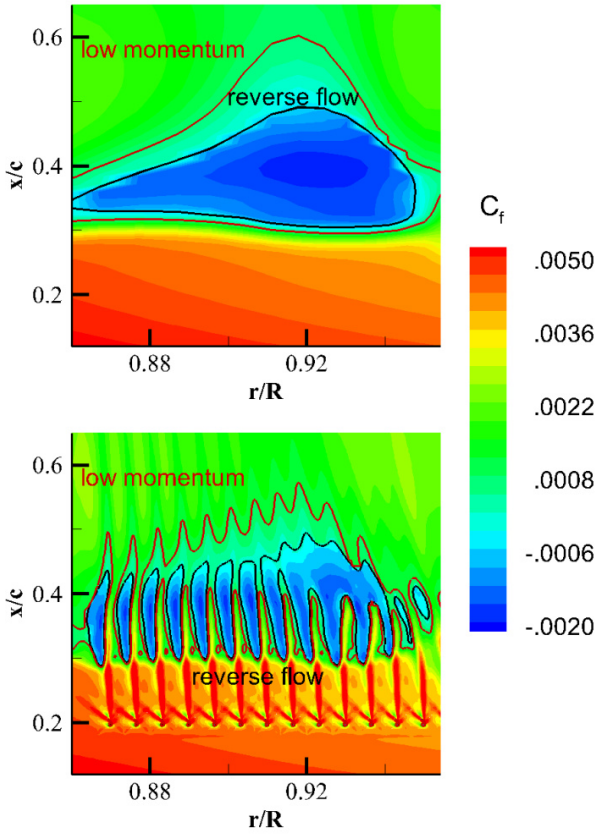

Figure 12. The effect of RVGs on the separation bubble and skin friction coefficient (ref. vs RVG).

The $\Delta M^2 C_n$ defined as the difference between the flow control and reference cases is presented in figure 14. The positive contribution (red color) of the proposed rod vortex generators appears at almost all azimuthal positions of the blade. The only negative effect (blue color) in terms of a normal force is present near ψ = 0˚

where the flow is separated starting already at the leading edge. The most benefits in the application of rods in the high-speed case of the AH-1G helicopter rotor are at ψ = 30˚ where a strong shock wave induces flow separation. The effectiveness in delaying shock induced flow separation by streamwise vortex generators have been already proven for channel flows[26] and is confirmed here for helicopter rotor blades as well. Although it is not as significant as for ψ = 30˚, the positive gain in normal force from ψ = 30˚ to ψ = 270˚ is also evident. Even without flow separation, the implementation of RVGs has a beneficial effect on the aerodynamic performance of the rotor blades. Low momentum areas are susceptible to flow separation and the application of flow control in such regions leads to a positive effect on normal force coefficient.

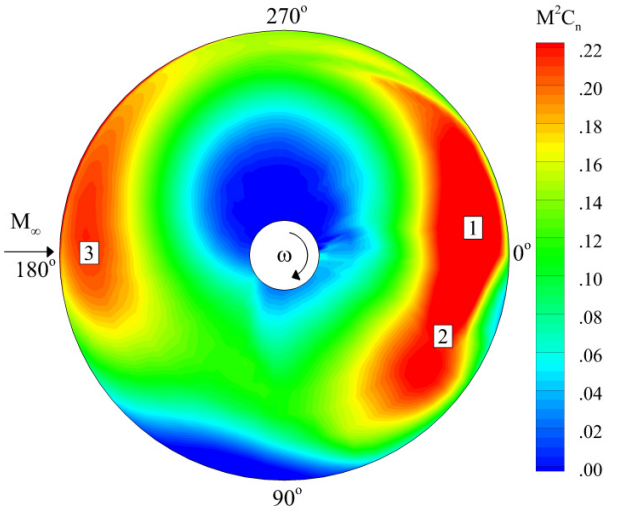

Figure 13. Disk loading for high-speed forward flight (AH-1G)

The Mach number contour maps at r/R = 0.92 at three cross-sections marked in figures 13 and 14 are presented in fig. 15. The first plot represents a massive flow separation due to high inflow angle. RVGs are creating streamwise vortices in an already reversed flow and large aerodynamic improvement cannot be expected. The second plot represents a high inflow velocity with a shock wave which induces flow separation. Lastly, the third plot is prepared for an intermediate state of flight where there is no flow separation but the boundary layer is disturbed by shock wave. The flow is more stable in the critical area close the wall and the normal force is slightly increased.

An average $\Delta M^2C_n/M^2C_{n\text{-REF}}$ in the rod vortex generators location reveals an enhancement of more than 7% in normal force coefficient. The numerical results concerning the application of rod vortex generators on helicopter rotor blades in forward flight presented in the paper confirm this technology as possible candidate to be integrated in the next generation of helicopters.

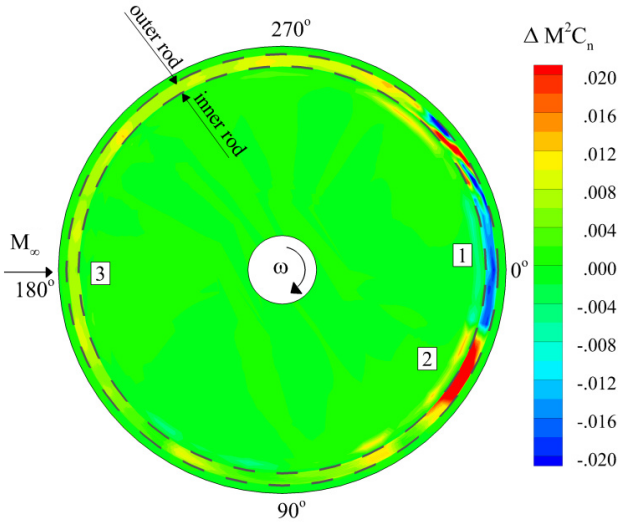

Figure 14. Effect of RVGs on the disk loading for high-speed forward flight (AH-1G)

5. CONCLUSIONS

The paper presents the details of numerical simulations of flow past helicopter rotor blades in hover and forward flight. The numerical models are validated against the experimental data / flight test data with a satisfactory agreement. The application of the own invention of rod vortex generators have been analyzed. The numerical results confirm the technology is improving the aerodynamic performance in both states of flight. As a first approach, the rods were continuously deployed which is valid for hover (quasi-steady flow) but can be improper for forward flight (unsteady flow). Although the application of RVGs in forward flight provides an average benefit in thrust, there are limited azimuthal locations where the flow is not improved. For this reason, the active deployment of RVGs as a function of the azimuthal position will be analyzed.

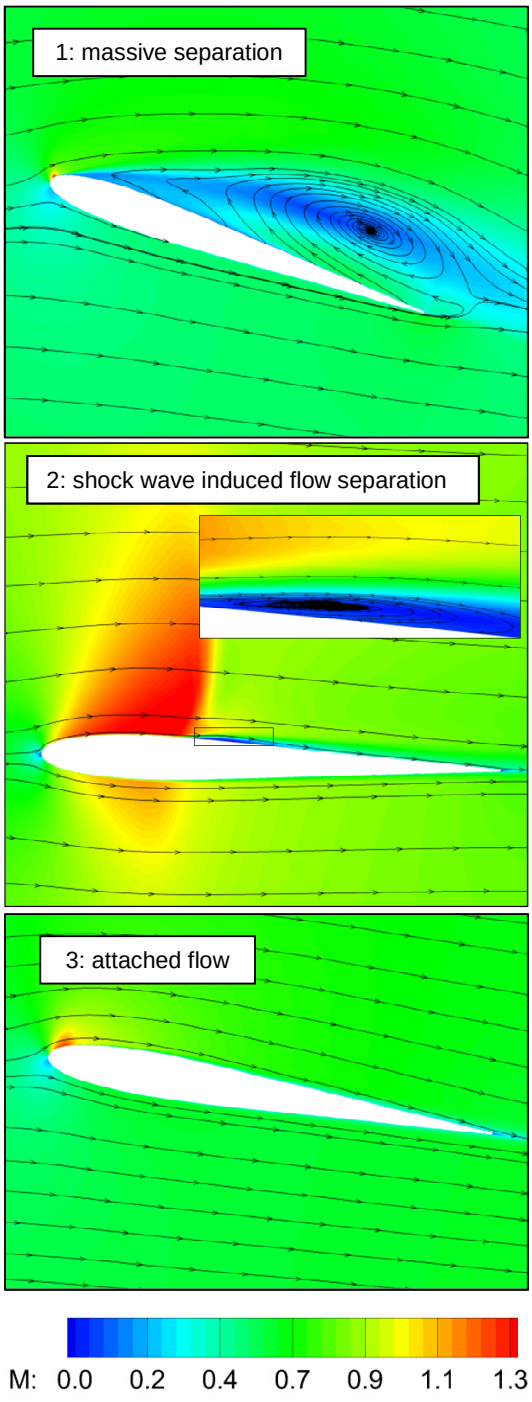

Figure 15.Flow structure for different azimuthal positions

REFERENCES

[1] Taylor H.D.: *The elimination of diffuser separation by vortex generators*. United Aircraft Corporation Report No. R-4012-3, June 1947

[2] Schubauer G.B. and Spangenber W.G.: *Forced mixing in boundary layer*. J. Fluid Mech., 1 1960. 8:10-32

[3] Bragg M.B. and Gregorek G.M.: *Experimental study of airfoil performance with vortex generators*. J Aircraft 1987; 24(5):305-9

[4] Brown A.C., Nawrocki H.F. and Paley P.N.: *Subsonic diffusers designed integrally with vortex generators*. J. Aircraft 1968; 5(3):221-9

[5] Wallis R.A.: *A preliminary note on a modified type of air jet for boundary layer control*. Aeronautical Research Council, Rept. CP 513, London, 1960

[6] Wallis R.A., Stuart C.M.: *On the control of shock-induced boundary layer separation with discrete air jets*. Aeronautical Resarch Council, Rept. CP 595, London, 1962

[7] Krzysiak A.: *Helicopter retreating blade stall control using self-supplying air jet vortex*.: *Proceedings of the 28th International Congress of the Aeronautical Sciences*. Brisbane (Australia) 2012

[8] Szwaba R., Flaszynski P., Szumski J. and Telega J.: *Shock wave – boundary layer interaction control by air-jet streamwise vortices.* Proceedings of the 8th International Symposium on Experimental and Computational Aerothermodynamics of Internal Flows. Lyon (France) 2007

[9]F.L.Tejero E. and Doerffer P.: *Numerical investigation of flow separation using air jet vortex generators on NACA0012 for transonic conditions*. Proceedings of the Congress on Numerical Methods in Engineering. Bilbao (Spain) 2013

[10] F.L. Tejero E., Doerffer P. and Szulc O.: *Effect of passive air jet vortex generator on NACA0012 performance*. Proceedings of the 5th European Conference for Aeronautics and Space Sciences, Munich (Germany) 2013

[11] Rao D.M. and Kariya T.T.: *Boundary-layer submerged vortex generators for separation control – an exploratory study*. AIAA Paper 88-3546-CP, AIAA/ASME/SIAM /APS 1st National Fluid Dynamics Congress, Cincinnati, OH, July 25-28, 1988

[12] Lin J.C.: *Review of research on low-profile vortex generators to control boundary-layer separation*. Progress in Aerospace Sciences 38 (2002) 389-420

[13] Doerffer P., Flaszynski P. and Szwaba R., 2009 Polish Patent P.389685

[14] Caradonna F.X. and Tung C.: *Experimental and analytical studies of a model helicopter rotor in hover*, NASA Technical Memorandum 81232 (1981)

[15] Cross J.L., Watts M.E.: *Tip aerodynamics and acoustic test*, NASA Reference Publication 1179

[16] Rossow C.C., Kroll N. and Schwamborn D.: *The MEGAFLOW project – numerical flow simulations for aircraft*. In: Di Bucchianico, A., Mattheij, R. M. M., Peletier, M. A. (eds.), Progress in Industrial

Mathematics at ECMI 2004, vol. 8, pp. 3-33, Springer, 2006
[17] Rung T., Lübcke H., Franke M., Xue L., Thiele F. and Fu S.: *Assessment of explicit algebraic stress models in transonic flows*. Proceedings of the 4th International Symposium on Engineering Turbulence Modelling and Measurements, Ajaccio (France) 1999.
[18] Schwarz T.: *The overlapping grid technique for the time accurate simulation of rotorcraft flows*. Proceedings of the 31st European Rotorcraft Forum, Florence (Italy) 2005
[19] Srinivasan G.R.: *A free-wake Euler and Navier-Stokes CFD method and its application to helicopter rotor inducing dynamic stall*. JAI Associates, Technical Report 93-01 (1993)
[20] Kang, H.J. and Kwon, O.J.: *Unstructured mesh Navier-Stokes calculations of the flowfield of a helicopter rotor in hover*. J. of the American Helicopter Society 47(2),90-99 (2002)
[21] Sun, H. and Lee, S.: *Response surface approach to aerodynamic optimization design of helicopter rotor blade*. J. Numer. Meth. Engng. 64, 125-142 (2005)
[22] Song, W.P., Han, Z.H. and Qiao, Z.D.: *Computational aeroacoustic prediction of transonic rotor noise based on Reynolds-Averaged Navier-Stokes flow simulation*. Proceedings of the 25th Congress of the International Council of the Aeronautical Sciences, Paper ICAS 2006-2.10.3, Hamburg (Germany) 2006
[23] Xu, J.H., Song, W.P. and Xie, F.T.: *Application of high-resolution scheme in rotor flow simulation*. Proceddings of the 27th Congress of the International Council of the Aeronautical Sciences, Paper ICAS 2010-2.1.3, Nice (France) 2010
[24] Doerffer, P. and Szulc O.: *Numerical simulation of model helicopter rotor in hover*. TASK Quaterly, vol. 12, no. 3, 2008.
[25] Doerffer P., Szulc O., Tejero E., F. L., Martinez S., J.: *Aerodynamic and aero-acoustic analysis of helicopter rotor blades in hover*. In: Bubak, M., (ed.), E-science on Distributed Computing Infrastructure: PLGrid Plus, LNCS, Springer, 2014
[26] Flaszyński P. and Tejero E. F. L.: *RANS numerical simulation of effectiveness of vortex generators in a curved wall nozzle*, *IMP PAN Report No. 365/2013 (in polish)*, Institute of Fluid-Flow Machinery, Poland, 2013.
[27] Hernandez F. and Johnson W.: *Correlation of airloads on a two-bladed helicopter rotor*. International Specialist Meeting on Rotorcraft Acoustics and Rotor Fluid Dynamics. PA. Oct. 1991.
[28] Ramachandran K., Schlechtriem S., Caradonna F.X. and Steinhoff J.S.: *Free-wake computation of helicopter rotor flowfield in forward flight*. AIAA paper 93-3079. July 1993
[29] Ahmad J. and Duque P.N.: *Helicopter rotor blade computation in unsteady flows using moving overset grids*. Journal of Aircraft, volume 33, number 1, pp 54-60
[30] Doerffer, P., Tejero E., F. L. and Szulc, O. *Numerical simulation of AH-1G helicopter rotor in forward flight using chimera overlapping grids technique*, *IMP PAN Report No. 105/2014*, Institute of Fluid-Flow Machinery, Poland, 2014.
[31] Szulc O., Doerffer P., Zoltak J., Malecki J.: *Time-accurate simulation of flow past PZL W-3A "Sokół" (Falcon) helicopter main rotor in forward flight*, Task Quarterly 17 No 1-2, pp 43-61

Acknowledgments
This work was supported by the 7th Framework Programme projects IMESCON (Grant Agreement PITN-GA-2010-264672) and STADYWICO (FP7/2007-2013 under grant agreement no. 251309). This research was supported in part by PL-Grid Infrastructure

The author(s) confirm that they, and/or their company or organisation, hold copyright on all of the original material included in this paper. The authors also confirm that they have obtained permission, from the copyright holder of any third party material included in this paper, to publish it as part of their paper. The author(s) confirm that they give permission, or have obtained permission from the copyright holder of this paper, for the publication and distribution of this paper as part of the ERF2014 proceedings or as individual offprints from the proceedings and for inclusion in a freely accessible web-based repository.